Article

The Effect of Ligand Electronics on the Reversible Catalytic Hydrogenation of CO to Formic Acid using Ruthenium Polyhydride Complexes: A Thermodynamic and Kinetic Study

Deven P. Estes, Markus Leutzsch, Lukas Schubert, Alexis Bordet, and Walter Leitner

ACS Catal., **Just Accepted Manuscript** • DOI: 10.1021/acscatal.0c00404 • Publication Date (Web): 31 Jan 2020

The Effect of Ligand Electronics on the Reversible Catalytic Hydrogenation of CO_2 to Formic Acid using Ruthenium Polyhydride Complexes: A Thermodynamic and Kinetic Study

Deven P. Estes,*[a,d] Markus Leutzsch,[c] Lukas Schubert,[a] Alexis Bordet,[a] Walter Leitner.*[a,b]

a) Max Planck Institute for Chemical Energy Conversion, Stiftstraße 34-36, Mülheim an der Ruhr, 45470, Germany.

b) Institute for Technical and Macromolecular Chemistry, RWTH Aachen, Worringerweg 2, Aachen, 52074, Germany.

c) Max Planck Institute for Coal Research, Kaiser-Wilhelm Platz 1, Mülheim an der Ruhr, 45470, Germany.

Keywords: reversible CO_2 hydrogenation, ruthenium polyhydrides, linear free energy relationships, CO_2 insertion kinetics, CO_2 insertion thermodynamics

Supporting Information Placeholder

ABSTRACT: Hydrogenation of CO_2 to formic acid or formates is often carried out using catalysts of the type $H_4Ru(PR_3)_3$ (**1**). These catalysts are also active for the reverse reaction, i.e. decomposition of formic acid to H_2 and CO_2. While numerous catalysts have been developed for the reactions in both directions, the detailed factors controlling the elementary steps of the catalytic cycle remain poorly understood. In this work, we synthesize a series of compounds of the type $H_4Ru(P(C_6H_4R)_3)_3$ containing both electron donating and electron withdrawing groups and analyze their influence on the kinetic and thermodynamic parameters of CO_2 insertion and deinsertion. The data are correlated with the catalytic performance of the complexes through linear free energy relationships. The results show that formic acid dissociation from the catalyst is rate-determining during CO_2 hydrogenation, while deinsertion is critical for the decomposition reaction.

Introduction

Complexes of the type $H_4Ru(PR_3)_3$ are a representative subgroup of the larger family of Ru phosphine catalysts for CO_2 hydrogenation and were among the first reported by Inoue.[1] The reaction of $H_4Ru(PPh_3)_3$ with CO_2 to form a κ^2-formate complex, the key elementary step for the initial C–H bond formation, is rapid and nearly thermoneutral.[2] Catalysts based on the related Ru(triphos) system hydrogenate CO_2 not only to formate but also to formaldehyde derivatives and even methanol.[3] This makes this catalyst family one of the most versatile homogeneous catalyst systems for CO_2 reduction.[3-4] At the same time, complexes of this type are also well known as catalysts for the reverse reaction, the decomposition of formic acid to H_2 and CO_2.[5] The reversibility of the reaction has been suggested as potential basis for hydrogen storage systems.[6, 1e] In particular, it is also a crucial factor in production schemes for formic acid as a chemical product, where the back reaction has to be suppressed or at least minimized in downstream processing.[7]

While numerous studies have measured the effect of ligand properties on CO_2 hydrogenation activity, relatively few studies have been able to rationalize the reasons for these ligand effects mechanistically in terms of the elementary steps. Jessop and coworkers screened over 24 monodentate phosphines at a 3:1 P:Ru ratio for their performance in CO_2 hydrogenation to formic acid.[1c] They found that, while more sterically hindered phosphines have lower activity, there was no simple correlation between phosphine basicity and activity. The basic mechanistic picture for transition metal catalyzed CO_2 hydrogenation to formic acid is well established.[8] Initial CO_2 insertion into a M-H bond is followed by H_2 activation by either an oxidative addition or heterolytic mechanism (σ-bond metathesis or 1–2 addition).[9] Finally, production of formic acid/formate takes place *via* either reductive elimination or dissociation, respectively, with concomitant regeneration of the active metal hydride species. Following the principle of microscopic reversibility, the reverse reaction, namely the catalytic decomposition of HCO_2H to H_2 and CO_2,[10, 1e] is generally assumed to occur via similar intermediates. However, a detailed fundamental understanding of the electronic factors that control these elementary steps is still lacking.

In this paper, we synthesize a series of $H_4Ru(P(p\text{-}C_6H_4R)_3)_3$ complexes with various electron donating and withdrawing groups in the para position of the aromatic phosphines. This allows us to vary the electronic properties of the ligand while keeping steric factors constant. We then study the effect of the ligand's electronic properties on the overall rate of formation and decomposition of HCO_2H. In addition, we also measure the thermodynamics and kinetics of the CO_2 insertion/de-insertion elementary step for all the complexes, which both of these reactions have in common. Our measurements show that the catalytic activity in both directions increases with increasing electron density before falling off at higher electron density. The thermodynamics and kinetics of the reversible CO_2 insertion corroborated by DFT analysis indicate that CO_2 hydrogenation is controlled by the activation energy of formic acid dissociation, while, for formic acid decomposition (under acidic conditions), CO_2 deinsertion from the formate intermediate appears to be rate limiting.

Results and Discussion

The synthesis of $H_4Ru(P(p\text{-}C_6H_4R)_3)_3$ where R = H (**1a**), CH_3 (**1b**), OMe (**1c**), CF_3 (**1d**) is accomplished using a modification of Chaudret's method:[11] reacting Ru(cod)(cot) with an excess of H_2 (2 bar) and three equivalents of the desired phosphine (figure 1). These polyhydride complexes are air and temperature sensitive and unstable to vacuum. They can, however, be precipitated out of the reaction solution using a non-polar solvent, filtered, and dried in a stream of argon. Substitution of the ligand at the para position increases solubility. Precipitation of complexes **1b** and **1d** is only possible using the very non-polar solvent hexamethyldisiloxane (HMDSO), which is key to their isolation as pure materials. All complexes show similar characterization data to complex

Table 1. Kinetics and thermodynamics for reaction of CO_2 with compounds **1a-d** and comparison to DFT calculations.

Compound	K_{eq} (313 K)	ΔH^{o}_{rxn}[a]	ΔS^{o}_{rxn}[b]	k_{ins} (313 K)[c]	k_{deins} (313 K)[c]	TOF (CO_2)[d]	TOF (FA) (s^{-1})[e]
1a (R = H)	1.16(1)	-2.5(1)	-7.8(5)	3.7(8)	2.9(6)	11 h^{-1} (3×10^{-3} s^{-1})	1.1
1b (R = CH_3)	1.83(3)	-3.0(1)	-8.5(2)	7.2(8)	4.2(5)	46 h^{-1} (13×10^{-3} s^{-1})	4.3
1c (R = OMe)	6.2(2)	-4.4(3)	-10.6(9)	7(1)	1.3(2)	5 h^{-1} (2×10^{-3} s^{-1})	0.36
1d (R = CF_3)	0.50(2)	-2.6(3)	-10(1)	< 0.4[e]	< 0.4[e]	2.5 h^{-1} (0.7×10^{-3} s^{-1})	0.0047

a) units of kcal mol^{-1}. b) units of cal $mol^{-1}K^{-1}$. c) units of s^{-1}. d) 2:1 1,4-dioxane:water, 0.34 M KOH, 40 °C, 30 bar each of H_2 and CO_2, catalyst conc. 0.0015 M, TON and TOF measured at 3h. e) 2:1 1,4-dioxane: water, 0.41 M FA, 40 °C, catalyst conc. 0.00083 M.

1a.[12, 1d] Their ^{1}H NMR spectra have only one signal in the hydride region (-6.9 – -7.4 ppm) and one signal in their ^{31}P NMR (58 – 53 ppm), suggesting that the phosphines and hydrides rapidly exchange on the NMR timescale, as has been observed for similar complexes.[13] Full characterization is shown in the SI (Figures S1-S10). The T1 values of the hydride signals of **1a-d** range from 65-70 ms at 40 °C (Table S3), suggesting that these are non-classical hydrides.[14] This is in agreement with DFT calculations showing that the tetrahydride form of **1a** (RuH_4) is 2.5 kcal mol^{-1} higher in energy than the dihydride hydrogen complex ($RuH_2(H_2)$).

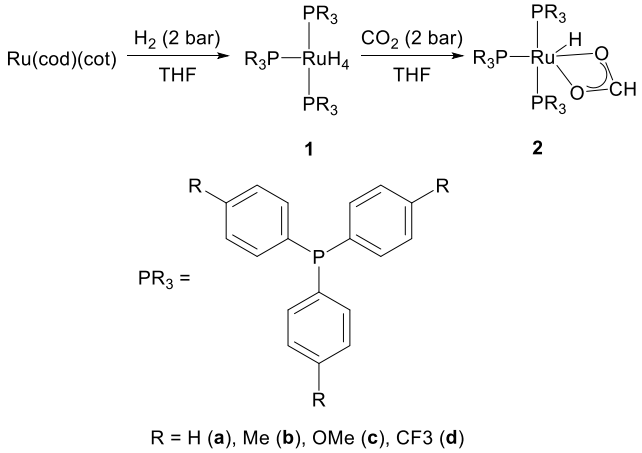

R = H (**a**), Me (**b**), OMe (**c**), CF3 (**d**)

Figure 1. Synthesis of **1a-d** and **2a-d**.

Complexes $HRu(OOCH)(P(C_6H_4R)_3)_3$ (R = H (**2a**), CH_3 (**2b**), OMe (**2c**), CF_3 (**2d**)) are made by reacting the crude solution described above with CO_2 (2 bar). These κ^2-formate complexes are also unstable under vacuum and at high temperatures and must be isolated by the same procedure as **1**. The characterization of these complexes is also analogous to those of complex **2a**. Their ^{1}H NMR spectra show signals corresponding to Ru–H (−17 - −19 ppm, quartet, $J_{P\text{-}H}$ = 26 – 28 Hz) and OOCH protons (8.5 - 7.9 ppm). Their ^{31}P NMR spectra show two signals at around 75 ppm (triplet, J = 28 Hz) and 42 ppm (doublet, J = 28 Hz) corresponding to phosphines in the equitorial and axial positions, respectively, that do not exchange rapidly on the NMR timescale. Bands at around 1550 and 1360 cm^{-1} in the IR spectrum confirm the presence of a κ^2-formate ligand. Full characterization is given in the SI (Figures S11-S21). Attempts to crystallize complexes **1b-d** and **2b-d** yielded hydride bridged dimeric species (see Figure S22).

$$CO_2 + H_2 \xrightarrow[2:1\ \text{dioxane:}H_2O,\ 40\ °C]{\text{KOH, } \mathbf{1}\ (0.44\ \text{mol\%})} HCO_2K + H_2O \quad (1)$$

$$HCO_2H \xrightarrow[2:1\ \text{dioxane:}H_2O,\ 40\ °C]{\mathbf{1}\ (0.2\ \text{mol\%})} CO_2 + H_2 \quad (2)$$

We tested the activity of **1a-d** in both the catalytic hydrogenation of CO_2 to give formate (under basic conditions, eq. 1) and the decomposition of formic acid (under acidic conditions, eq. 2). The complexes were active for hydrogenation of CO_2 even at ambient temperatures. Temperatures above 70 °C resulted in formation of Ru metal. Catalytic tests were carried out at 40 °C in a 2:1 mixture of 1,4-dioxane:water (for catalyst solubility) containing 0.34 M KOH with a catalyst loading of 0.44 mol% vs KOH (results shown in Tables 1 and S2). The CO_2 hydrogenation TOF increases with increasing electron donation from 2.5 h^{-1} for **1d** to 46 h^{-1} for **1b** before dropping in activity for **1c** (5.6 h^{-1}). Catalyst **1b** is more active than many other Ru complexes of the same family[1e] and operates at a much lower temperature. The measured TOF is zero order in [KOH], the limiting reagent, and has a first order dependence on the partial pressures of both CO_2 and H_2 (Table S2). Since the catalyst concentration and partial pressures $P(CO_2)$ and $P(H_2)$ are all constant during the reaction, the formation of [HCO_2K] is linear as a function of time. Measurement of the TOF at different times during the reaction shows no signs of deactivation after 240 turn overs. The decomposition of formic acid to CO_2 and H_2 was also performed at 40 °C in the same solvent mixture containing 0.41 M formic acid (0.2 mol% catalyst loading). The trend of the activity of formic acid decomposition is similar to that seen for CO_2 hydrogenation, where **1d**, **1a**, **1b**, and **1c** have TOFs of 0.0047, 1.1, 4.3, and 0.36 s^{-1}, respectively. This trend shows that as the ligands become more electron donating the catalytic activity increases up to a point, after which it falls off again. Complexes in the middle of the electron donor scale thus have the best activities for both CO_2 hydrogenation and formic acid decomposition

The reason for this unusual trend between electron density and catalytic activity is not immediately obvious. While ligand variation has been widely used to optimize catalyst performance for CO_2 hydrogenation, systematic studies of the effects of ligand electronics on the catalytic activity are limited. In the existing examples in the literature, linear free energy relationships (LFERs) are often used to determine the catalytically-relevant step and thereby explain the overall effect of electron density on catalytic activity. Appel and coworkers found that for a series of Co and Rh complexes better hydride donors (related to the electron donor ability of the ligands) also have faster turnover frequencies when hydrogenating CO_2 to formate in the presence of a base.[15] Hazari and Mayer found that increasing the hydricity of Ni–H pincer complexes (e.g. by making the metal center more electron rich) also increases the rate of CO_2 insertion.[16] This is also the case for some Ru pincer complexes.[17] However, Kubiak and coworkers showed that for a different series of Rh phosphine complexes, poorer hydride donors are better catalysts.[18] LFERs have also been computationally investigated both for a series of Fe and Co tripodal complexes[19] as well as for a large number of pincer species based on group 8 and 9 metals.[20] The conclusion of all of these studies is that the disparate dependencies of TOF on hydricity (electron donation from the ligands) for various systems is the result of a catalytic cycle in

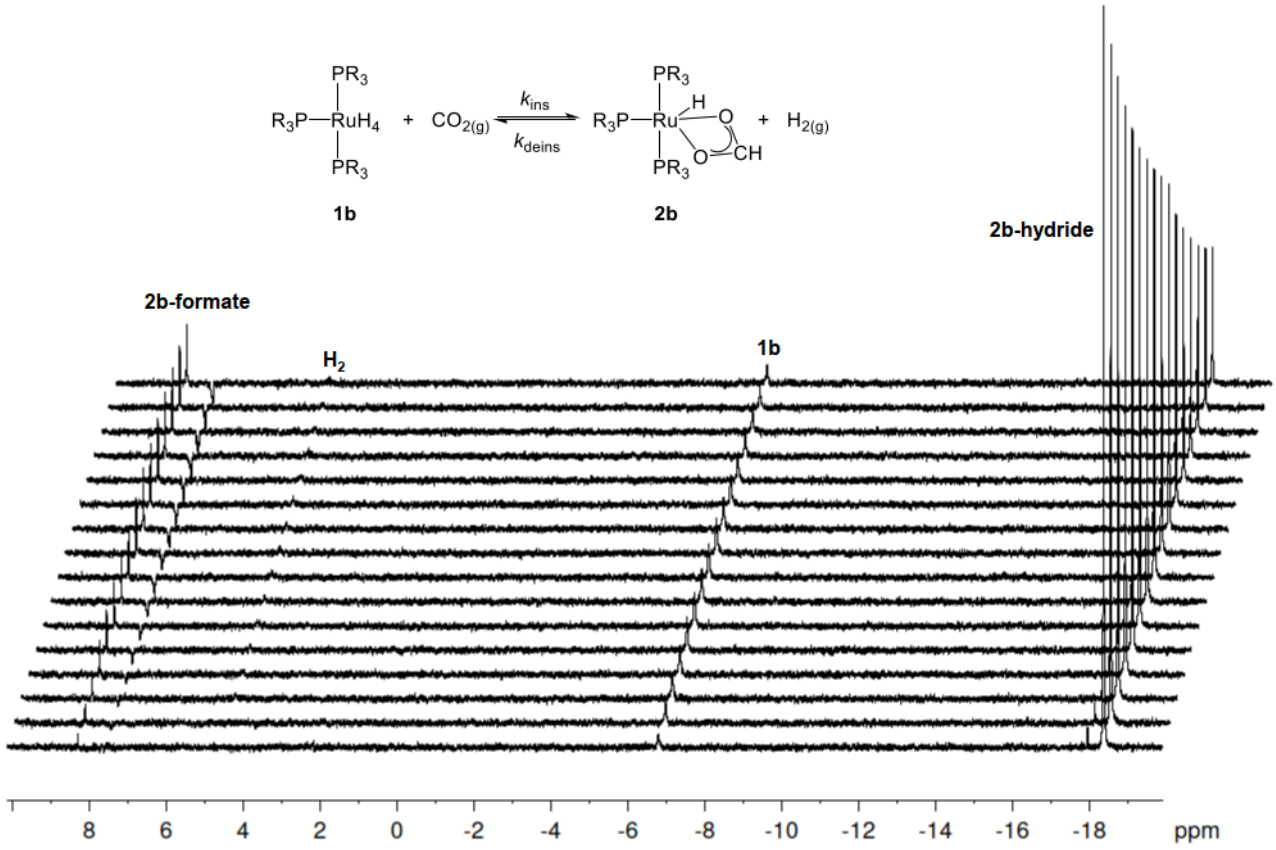

Figure 2. Selective EXSY experiment of **1b**/**2b** at 40 °C upon excitation of the hydride (mixing time 0.01 – 0.5 s) with positive phasing.

which either CO_2 insertion or H_2 activation is rate-determining. In the former case, more hydridic hydrides (with electron donor ligands) will result in increased TOF. If reformation of the M–H species is rate determining, then the opposite will be true. However, a trend in which complexes in the middle of the electron density scale have better activity than those on the extremes does not fall into either of these categories. In order to gain more direct experimental insight into the central elementary step for the CO_2 hydrogenation to formic acid and its decomposition, we measured the thermodynamics and kinetics of the reversible CO_2 insertion step for all four complexes **a-d** (eq. 3 and 4).

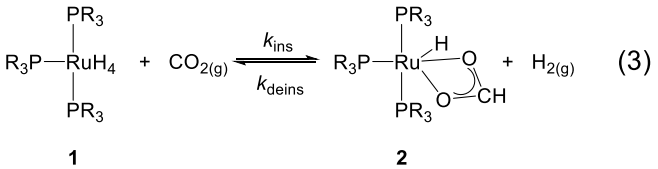

(3)

$$K_1 = \frac{k_{ins}}{k_{deins}} = \frac{[\mathbf{2}]P_{H_2}}{[\mathbf{1}]P_{CO_2}} \qquad (4)$$

As the equilibria shown in eq. 4 are known to lie relatively close to one and we have isolated both **1** and **2** in each case, we were able to determine the equilibrium constant K_1 by quantitative NMR spectroscopy. In order to accurately know the partial pressures of the two gases, we saturated the solution with a large excess of a mixture of 1:1 H_2:CO_2 at 1.4 bar in a J-Young NMR tube and then monitored the equilibrium starting from complexes **1** by ^{1}H NMR spectroscopy using ferrocene as an internal standard (Figures S28-S31). The equilibrium was also established starting from a solution of **2** in order to confirm that the same equilibrium was reached. The measured equilibrium constants are shown in Table 1.

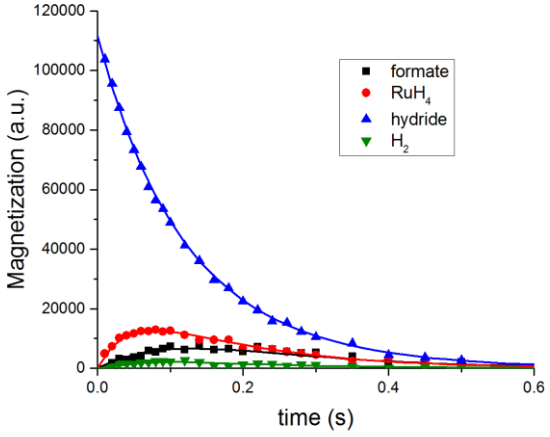

Figure 3. Selective EXSY of the **1b**/**2b** system at 40 °C upon excitation of the hydride signal of **2b**. (phased positively for easier analysis)

More electron donating ligands result in more thermodynamically favorable insertion of CO_2. Of the complexes here, reaction of CO_2 at 20 °C with **1c** is about 15 times more thermodynamically favorable than with **1d**. We also measured the equilibrium constant at different temperatures and thereby measured the enthalpy and entropy of reaction.

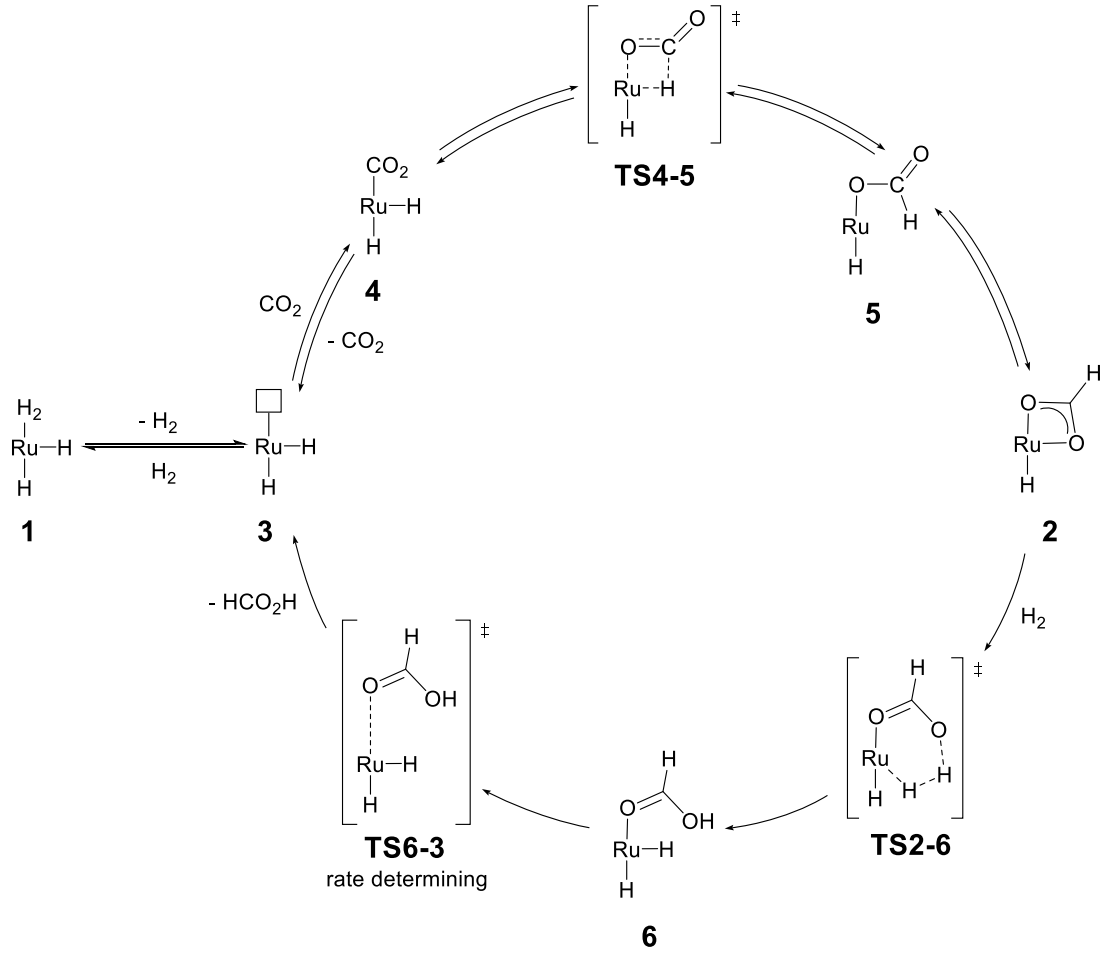

Figure 4. Plausible catalytic cycle for CO_2 hydrogenation catalyzed by **1a-d.**

These data are also shown in Table 1 (see Figures S32 - S35). The enthalpy of reaction becomes more negative upon going from electron withdrawing to electron donating ligands. The entropy of reaction also becomes more negative with more electron donating ligands. Complex **1d** gives both a ΔH^{o}_{rxn} and ΔS^{o}_{rxn} that are more negative than we would expect, based on the values of the other complexes. This may be due to differences in the vibrational entropy of complex **2d** (since other factors should be similar from reaction to reaction). The IR spectra of the formate complexes support this conclusion. The asymmetric formate stretch of **1d** (1543 cm^{-1}) is approx. 10 cm^{-1} lower than those of **1a-c** (1555-1551 cm^{-1}).

We next measured the rate of CO_2 insertion to see if more thermodynamically favorable insertions were faster. The insertion rate of CO_2 into complexes **1a-d** was too fast to measure easily by conventional reaction monitoring and too slow to measure by NMR line broadening. However, the exchange between species **1** and **2** can be observed using selective EXchange SpectroscopY (EXSY).[21] In this experiment, one peak in the ^1H NMR spectrum is selectively inverted. During a mixing time, this inversely magnetized proton is then transferred to other positions by chemical exchange. Varying the mixing time allows us to measure the concentration profiles of each exchange partner in the reaction and therefore extract rate constants for their interconversion. In order to measure the rate constants of CO_2 insertion and deinsertion, an equilibrium mixture of **1** and **2** was established by exposing a solution of either **1** or **2** in C_6D_6 to 1.4 bar of 50:50 H_2:CO_2 at 40 °C. Selected data from these experiments can be seen in figure 2 as well as figures S36 - S39. The EXSY NMR of this mixture showed magnetization transfer between both the hydride and formate positions of **2** as well as to **1** and to free H_2. The time profile of magnetization transfer for complex **1b** is shown as an example in Figure **3**.

We fit the magnetization data to a kinetic model using the Runge-Kutta method as implemented in the program Berkeley-Madonna.[22] The kinetic model as well as the fitted data are shown in the supporting information (Scheme S1, Table S3, Figures S40-S51). This model included steps for equilibration of **1** and **2**, exchange of **1** with H_2, and the T_1 relaxation of each proton (which were measured by separate inversion recovery experiments). The deinsertion rate constant was not directly modeled, but was instead fixed to the fitted value of the insertion rate constant using our measured equilibrium constant at 40 °C. An additional correction was necessary to account for loss of magnetization by the formation of para-H_2.[23] The results of fitting for each complex are shown above in Table 1. The final rate constants are the averages of those obtained from individual irradiation of each exchanging signal.

While complexes **1a-c** have insertion rates on the order of 3 - 7 s^{-1}, the most electron poor complex, **1d**, showed no exchange faster than relaxation at 40 °C. When either the formate or hydride of **2** was irradiated, buildup of magnetization into tetrahydride **1** precedes exchange into the other position of **2**. This indicates that the exchange between the formate and hydride positions of **2** happens via the intermediacy of **1**. The insertion rates depend neither on the concentration of complex (unimolecular) nor on the concentration of the gas mixture. This is expected for the deinsertion and suggests that insertion is preceded by dissociative substitution of coordinated H_2 by CO_2.In order to correctly model the data for complex **1c**, an additional step was necessary in the model

in which the formate and hydride of **2** can directly exchange, without going to **1**. This step (rate constant k_{exch}) was modeled for all complexes but played little to no role in the fits of complexes **1a** and **1b** (result of fitting was not sensitive to changes in k_{exch}). This suggests that the presumed CO_2 complex (**4c**) is long-lived enough to allow it to directly reinsert CO_2 to reform **2c**, resulting in overall exchange without the intermediacy of **1c**. For complex **2c**, k_{deins} and k_{exch} are equal, which supports this hypothesis. The fact that this direct exchange is not important for complexes **1a** and **1b** is likely due to the fact that CO_2-complexes **4a** and **4b** are very short-lived and quickly expel CO_2.

More electron-rich complexes do indeed result in faster insertion up to a point, after which the rate of insertion no longer increases. The insertion rates of CO_2 show the same trend as we see for catalytic activity, with **1b** having both the fastest TOF and the highest rate of insertion. However, the measured rates of CO_2 insertion are roughly three orders of magnitude faster than catalysis. This suggests that CO_2 insertion is not the rate determining step for the forward reaction. This would explain why we do not see a similar LFER to those observed for cases when CO_2 insertion is rate determining.

If CO_2 insertion plays little to no kinetic role in the overall rate of CO_2 hydrogenation, then what is the kinetically relevant step of catalysis? Looking more closely at the mechanistic evidence will help us answer this question. We found that CO_2 hydrogenation is 1st order in both $P(H_2)$ and $P(CO_2)$ and 0th order in [KOH] (Table S2), suggesting that the rate-determining step occurs after CO_2 insertion and H_2 activation but before deprotonation. We also found that the TOFs are not dependent on solvent or base. The TOF of **1a** in toluene with 0.34 M NEt_3 as base is also 0.003 s^{-1}. These data are consistent with a mechanism in which formic acid dissociation from the complex is rate-determining (**TS6-3**, Figure 4). Such a mechanism has been proposed previously for certain Rh and Ru catalysts that are also 1st order in both H_2 and CO_2 and 0th order in base.[24] Rate-determining formic acid dissociation might also explain the trend of catalytic activity. Formic acid can more easily dissociate from electron rich catalysts (i.e. more electron rich catalysts have a lower barrier for dissociation), making them more active. However, for very electron rich catalysts, such as **1c**, the increased stabilization of the resting state **2c** may result in an overall increased barrier for formic acid dissociation from **2c** and lower catalytic activity than for **2b**. Another explanation for the low TOF of **2c** could be a change in rate determining step. As the complexes become more electron rich, formic acid dissociation will become more favored (lower energy for the final **TS6-3** in figure 4), while H_2 activation (through transition state **TS2-6**) will become disfavored. It is possible that the energy of **TS2-6** for **2c** thus becomes the largest energy barrier along the pathway. Such a mechanism would still agree with our experimental data and explain the different behavior of **2c**.

Based on this mechanism, we would expect much faster rates for formic acid decomposition, since formic acid dissociation no longer plays a role. Indeed, the rates of catalytic formate decomposition and the rate constants of CO_2 elimination are on the same order of magnitude and follow the same trend in terms of ligand electronics. This suggests that CO_2 elimination is the limiting step during formic acid dehydrogenation. The rate law, which is 1st order in formic acid over four half-lives (Figure S23), also supports this hypothesis. Such a rate law is consistent with a mechanism in which pre-equilibrium association of formic acid with the catalyst is followed by rate-determining elimination of CO_2 from the intermediate formate complex.

In conclusion, Ru complexes of the type $H_4Ru(PR_3)_3$ are good catalysts for both the hydrogenation of CO_2 and the decomposition of formic acid under mild conditions. Varying the electron donor properties of the ligands shows that mildly electron-donating phosphines give the highest activities. The thermodynamics and kinetics of the insertion of CO_2 into **1** suggest that CO_2 insertion plays little role in catalysis. The difference in reactivity is likely due to variations in the rate of dissociation of formate caused by the ligands' electronic properties. These findings show the power of linear free energy relationships as useful mechanistic tools for determining the rate-limiting step of CO_2 hydrogenation catalysts. These findings also show that, in addition to CO_2 insertion and H_2 activation, formic acid dissociation from the catalyst can also play an important role in CO_2 hydrogenation.

Experimental

All experiments were carried out under dry and oxygen free argon using standard Schlenk and glovebox techniques. Pentane, THF, toluene, HMDSO, 1,4-dioxane, and deuterated benzene were purified by distillation over appropriate drying agents and degassed by argon-bubbling for at least 1h and was stored over molecular sieves. Air-free solutions in water were made by using a Milli-Q water purification system with resistivity of 18.2 MΩ•cm and less than 5 ppb TOC. Phosphine ligands, KOH, sodium benzoate, benzoic acid, H_2 (5.0 purity), CO_2 (4.8 purity), and a 1:1 mixture of H_2 and CO_2 (4.8 purity) were purchased and used as received. Ru(cod)(cot) was synthesized as previously reported.[25]

NMR spectra were measured on a 400 MHz Bruker Avance III spectrometer. ^{13}C NMR spectra and 2D NMR were measured on a 500 MHz Bruker AVIII spectrometer equipped with a liquid N_2 cryoprobe. Quantitative ^1H NMR spectra were measured using a recycle delay of 60 s in the presence of a known concentration of internal standard. The selective 1D EXSY/NOESY experiments were performed at a Bruker AVIII 300 MHz WB NMR spectrometer equipped with a 5 mm BBFO with z-gradient and a BCU cooling unit for temperature regulation. The temperature was calibrated with a sample of 80% ethylene glycole in DMSO-d_6.[26] IR spectra were measured using a Nicolet iS5 IR spectrometer with a Diamond ATR attachment inside of a glovebox. Elemental analyses were conducted by Mikroanalytisches Laboratorium Kolbe (Oberhausen, Germany).

Synthesis of Ru Complexes

*Synthesis of $H_4Ru(P(C_6H_4Me)_3)_3$ (**1b**)*

Polyhydrides of Ru were made by a modification of the procedure by Chaudret and coworkers.[11] Ru(cod)(cot) (50 mg, 0.16 mmol) and $P(C_6H_4Me)_3$ (140 mg, 0.46 mmol) was loaded into a Fisher-Porter bottle, dissolved in 2 mL THF, and stirred for 15 min giving a yellow solution. The Fisher-Porter bottle was then pressurized with 2 bar of H_2 and stirred at room temperature for 3h, after which time the solution had turned light orange. The desired complex was isolated from the reaction mixture by addition of 10 mL of HMDSO followed by storage of the material at -40 °C. The multicrystalline solid thus obtained was then filtered and dried under a flow of argon. This compound was an orange, temperature and air sensitive solid which based on NMR and elemental analysis was obtained as a 3:3:1 complex:THF:HMDSO adduct in the solid state, and was stored in a glovebox at -40 °C. The solvent could not be removed without destroying the complex. (120 mg, 74% yield) ^1H NMR (400 MHz, C_6D_6, δ) 7.56 (m, 18H), 6.79 (m, 18 H), 2.03 (s, 27H), –6.87 (br s, 4H). ^{13}C NMR (100.6 MHz, C_6D_6, δ) 138.9 (m), 137.3, 134.2 (m), 127.8 (overlapping with C_6D_6 peak), 20.7. $^{31}P\{^1H\}$ NMR (162 Hz, C_6D_6, δ) 55.8 (s). IR (ATR, cm^{-1}) ν_{max} = 3076, 3053, 3019, 2977, 2921, 2864 (C-H stretch), 1932 (H–Ru stretch). Elemental Analysis: Calc. 72.4 %C, 7.1 %H, 8.1 %P. Found 72.2 %C, 6.8 %H, 8.4 %P.

*Synthesis of $H_4Ru(P(C_6H_4OMe)_3)_3$ (**1c**)*

Same procedure as above. Addition of 10 mL of hexamethyldisiloxane (HMDSO) resulted in the formation of a redish precipitate, which was then filtered. This powder was then dried under flowing argon. This compound was a redish-orange temperature and air sensitive powder

and therefore stored in a glovebox at -40 °C. (111 mg, 60% yield) ^{1}H NMR (400 MHz, C_6D_6, δ) 7.55 (m, 18H), 6.60 (m, 18 H), 3.27 (s, 27H), –6.92 (br s, 4H). ^{13}C NMR (100.6 MHz, C_6D_6, δ) 159.8, 135.6 (m), 133.7 (m), 112.7 (m), 54.3. ^{31}P{^{1}H} NMR (162 Hz, C_6D_6, δ) 53.3 (s). IR (ATR, cm^{-1}) ν_{max} = 3068, 3004, 2951, 2902, 2834, (C-H stretch), 2046, 1921 (H–Ru stretch). Elemental Analysis: Calc. 64.0 %C, 6.1 %H, 7.6 %P, 1.83 %Si. Found. 63.3 %C, 5.5 %H, 7.5 %P, 1.83 %Si.

*Synthesis of $H_4Ru(P(C_6H_4CF_3)_3)_3$•THF (**1d**)*

Same procedure as above. The desired complex was isolated from the reaction mixture by addition of 10 mL of HMDSO followed by storage of the material at -40 °C. The multicrystalline solid thus obtained was then filtered and dried under a flow of argon. This compound is a yellow, temperature and air sensitive solid isolated as the 1:1 compound:THF adduct and stored in a glovebox at -40 °C. (110 mg, 68% yield) ^{1}H NMR (400 MHz, C_6D_6, δ) 7.09 (m, 18H), 7.01 (m, 18 H), –7.42 (br s, 4H). ^{13}C NMR (125.7 MHz, C_6D_6, δ) 142.6 (m), 133.5 (m), 131.6 (q, J = 32.7 Hz), 124.6 (m), 123.8 (q, J = 272.8 Hz). ^{31}P{^{1}H} NMR (162 Hz, C_6D_6, δ) 57.6. IR (ATR, cm^{-1}) ν_{max} = 3066 (C-H stretch), 1930 (br) (H-Ru stretch). Elemental Analysis: Calc. 51.1 %C, 3.1 %H, 5.9 %P. Found. 50.8 %C, 2.8 %H, 6.0 %P.

*Synthesis of $HRu(OOCH)(P(C_6H_4Me)_3)_3$•PhMe (**2b**)*

Ru(cod)(cot) (50 mg, 0.16 mmol) and $P(C_6H_4OMe)_3$ (150 mg, 0.43 mmol, 2.67 equiv) was loaded into a Fisher-Porter bottle, dissolved in 5 mL THF, and stirred for 15 min giving a yellow solution. The Fisher-Porter bottle was then pressurized with 2 bar of H_2 and stirred at room temperature for 3h, after which time the solution had turned light orange. The gas phase was then removed with vacuum and the bottle filled with 2 bar of CO_2 under vigorous stirring. The solution turned darker orange almost immediately. This was stirred for 2h. We bubbled a stream of CO_2 through the crude solution to concentrate it to one third of its original volume. To this concentrated solution was added 20 mL of pentane to form a slightly cloudy solution. This was placed at -78 °C causing a precipitate to form from the solution. This was then filtered, washed with pentane at -78 °C (3x4 mL), and dried under a stream of CO_2 for 30 min to give a pure yellow powder. 40 mg, 24% yield. Stored at -35 °C in a glovebox. Alternatively, this crude product could be recrystallized by vapor diffusion of pentane into a concentrated toluene solution at -35°C. Recrystallized material obtained as the toluene adduct in the solid state. ^{1}H NMR (400 MHz, C_6D_6, δ) 8.25 (1H, s), 7.52 (m, 18H), 6.85 (d, J = 8 Hz 12 H), 6.71 (d, J = 8 Hz, 6 H), 2.05 and 2.03 (overlapping s, 27H), –18.41 (q, J_{P-H} = 26.7 Hz, 1H). ^{13}C NMR (125.7 MHz, C_6D_6, δ) 172.2, 137.9, 137.6, 135.3 (d, J = 45.2Hz), 135.0 (vt, J_{app} = 5.7 Hz), 134.5 (d, J = 10.0 Hz), 134.1 (vt, J_{app} = 18.8 Hz), 127.9, 127.4 (these two resonances are hidden under the C_6D_6 signal but are visible in the HMBC spectrum shown below), 20.9, 20.8. ^{31}P{^{1}H} NMR (162 Hz, C_6D_6, δ) 76.4 (td, J = 29 Hz, J = 5.4 Hz), 42.0 (dd, J = 28.3 Hz, J = 5.7 Hz). IR (ATR, cm^{-1}) ν_{max} = 3064, 3008, 2927 (C-H stretches), 2836 (H-COORu stretch), 1551 (HCOO sym), 1362 (HCOO asym). Elemental Analysis: Calc. 74.0 %C, 6.4 %H, 8.1 %P. Found 73.6 %C, 6.7 %H, 8.3 %P.

*Synthesis of $HRu(OOCH)(P(C_6H_4OMe)_3)_3$•1/2 HMDSO (**2c**)*

Same procedure as above. The compound was then precipitated out of the concentrated THF solution by addition of HMDSO. This powder was then dried in a flow of CO_2. The product was obtained as 2:1 adduct with HMDSO. This compound was temperature and air sensitive and therefore stored in a glovebox at -35 °C. In some cases, the product still contained some impurities after this procedure. These could be removed by recrystallizing by slow vapor diffusion of pentane into a saturated toluene solution at -35 °C (the NMRs shown below are after pentane/toluene crystallization). (107 mg, 56% yield) ^{1}H NMR (400 MHz, C_6D_6, δ) 8.49 (1H, s), 7.81-7.46 (m, 18H), 6.68-6.52 (m, 18 H), 3.30-3.29 (overlapping s, 27H), –18.52 (q, J_{P-H} = 28 Hz, 1H). ^{13}C NMR (125.7 MHz, C_6D_6, δ) 172.2, 160.2, 160.0, 136.3 (vt, J_{app} = 6.3Hz), 135.8 (d, J = 11.3), 129.0 (vt, J_{app} = 21.4), 112.8 (vt, J_{app} = 5 Hz), 112.3 (d, J = 10 Hz), 54.3, 54.2. ^{31}P{^{1}H} NMR (162 Hz, C_6D_6, δ) 74.5 (t, J = 29 Hz), 39.2 (d, J = 28 Hz). IR (ATR, cm^{-1}) ν_{max} = 3066, 2997, 2935, 2902 (C-H stretch), 2834 (H-COORu stretch), 1554 (HCOO sym), 1361 (HCOO asym). Elemental Analysis: Calc. 62.6 %C, 5.8 %H, 7.2 %P. Found 62.7 %C, 5.3 %H, 7.5 %P.

*Synthesis of $HRu(OOCH)(P(C_6H_4CF_3)_3)_3$•1/4HMDSO (**2d**)*

Same procedure as above. To the concentrated solution was added 20 mL of hexamethyldisiloxane (HMDSO) to form a slightly cloudy solution. This was placed at -78 °C freezing most of the solution with only a thin layer of liquid on top. This liquid was filtered off and the solution allowed to thaw, forming a yellow orange precipitate. This was then filtered, washed with more HMDSO (2x4 mL), and dried under a stream of CO_2 for 30 min to give a pure yellow powder that is soluble in pentane and sparingly soluble in HMDSO. More solid formed from the filtrate and washings and thus a second batch was isolated from the washings by filtration and drying under CO_2. Total yield 95 mg, 38% yield. Some HMDSO remained in the powder after isolation (the sample was approximately 20% HMDSO). Stored at -35 °C in a glovebox. ^{1}H NMR (400 MHz, C_6D_6, δ) 7.84 (1H, dt, J_1 = 2 Hz, J_2 = 4 Hz), 7.16-7.13 (m, overlapping with C_6D_6), 7.04 (m, 12 H), 6.97-6.91 (m, 12 H), –18.58 (q, J_{P-H} = 26.7 Hz, 1H). ^{13}C NMR (125.7 MHz, C_6D_6, δ) 174.3, 138.9 (d, J = 45.2 Hz), 138.0 (vt, J_{app} = 18.9 Hz), 134.4 (vt, J_{app} = 6.3 Hz), 133.7 (d, J = 10.0 Hz), 132.1 (q, J = 32.7 Hz), 132.0 (q, J = 32.7 Hz), 124.6 (m), 124.3 (m), 123.8 (q, J = 272.8 Hz), 123.6 (q, J = 272.8 Hz). ^{31}P{^{1}H} NMR (162 Hz, C_6D_6, δ) 76.4 (t, J = 27.5 Hz), 42.4 (d, J = 27.5 Hz). ^{19}F{^{1}H} NMR (376.5 Hz, C_6D_6, δ) –63.09, –63.22. IR (ATR, cm^{-1}) ν_{max} = 3072 (br) (Aromatic C-H stretch), 2808 (H-COORu stretch), 2002 (w, Ru-H stretch), 1543 (HCOO sym), 1363 (HCOO asym), 1398, 1320 (CF_3 stretch) 1172, 1125, 1109, 1054, 1017. Elemental Analysis: Calc. 49.6 %C, 2.7 %C, 5.9 %P Found. 49.1 %C, 2.7 %H, 5.9 % P.

Catalytic Reactions

Formic Acid Decomposition

Two mL of a degassed 1.23 M formic acid solution in water with benzoic acid as internal standard were added to a 4 mL solution containing 0.005 mmol of Ru catalyst that had been preheated to 40 °C. Samples (0.1 mL) were taken periodically, diluted in oxygenated D_2O (to oxidize the catalyst) and quantitative ^{1}H NMR measured immediately. The concentration of formic acid still in the solution, was determined by comparison with the internal standard. The reactions were first order in formic acid for at least four half-lives.

Base-Promoted Hydrogenation of CO_2

Caution: High-pressure experiments with compressed gases are dangerous and should only be carried out using suitable equipment and appropriate safety measures.

In a steel autoclave outfitted with a glass liner and magnetic stirbar, 0.006 mmol of **1** was dissolved in 2 mL of 1,4-dioxane. To this was added 1 mL of degassed 1M KOH in water. The autoclave was then pressurized with 30 bar each of H_2 and CO_2. The reaction was stirred at 40 °C for 17h and the progress checked by ^{1}H NMR spectroscopy using sodium benzoate as an internal standard. During this amount of time, the pressures in the autoclaves did not change. However, in the case of **1a** and **1b**, the amount of KOOCH visible in the solution suggested 100% conversion (complete consumption of KOH). Thus, these reactions were rerun and tested after only 3 hours. The conversion at these conditions

was less than 30%, allowing the use of the initial rates method. Changing both the pressure of H_2 and CO_2 resulted in a consequent first order change in the rate of reaction. Taking samples at different times showed that the reactions were also 1st order in KOH.

Equilibrium Measurements

Each compound (**1** and **2**) was weighed into a separate J-Young NMR tube (approximately 10 mg) along with a known amount of internal standard (ferrocene, 10 mg) and 0.6 mL of C_6D_6. This mixture was then frozen in a salt water - ice bath (–20 °C), the atmosphere removed under vacuum, and filled with 1.4 bar of a 50:50 mixture of CO_2 and H_2. The solution was then thawed and thoroughly mixed with the gas phase. This process was repeated once more to ensure accurate partial pressures of the two gases. This mixture was then placed in the probe of a 400 MHz NMR spectrometer heated to the desired temperature and allowed to equilibrate for 10 min. After this equilibration time an NMR was measured (recycle delay 10 s) and the mixture was ejected from the NMR, mixed with the gas phase, and placed back in the probe to equilibrate for another 10 min. This process was repeated until the NMR spectrum was constant to ensure good equilibration of the gas and liquid phases at the desired temperature. Both samples were found to give the same values of equilibrium constant for each temperature to within a maximum of 7% error. The measurements were performed at 283K, 293K, 303K, and 313K and the average values of both the measurements starting from either **1** or **2** taken as the final value for the equilibrium constants at each temperature.

Selective 1D Exchange Spectroscopy (sEXSY) Measurements

Exchange rate constants were measured using a 1D EXSY/NOESY experiment.[27] For this experiment, the standard sequence from the BRUKER library (selnoegp) was used and modified to a pseudo-2D version to measure different exchange times in one experiment and decouple ^{31}P during acquisition. The standard proton $\pi/2$ pulse length was 14 μs. For selective inversion of the hydride signal a 5.2 ms Gaussian shaped π degree pulse was used. For the other resonances an 11 ms Gaussian shaped π degree pulse was used. Samples were prepared as above for the equilibrium measurements and warmed to 313 K, once again with successive equilibration and shaking of the tube to equilibrate the gas and liquid phases. Four separate EXSY experiments were then measured, in which the formate signal of **2** (8.2 ppm), the hydride signal of **2** (-18.5 ppm), the hydride signal of **1** (~-6.9 ppm), and H_2 (4.5 ppm) were successively excited. The evolution of the magnetization transfer was monitored after different exchange times (0.01 s, 0.02 s, 0.03 s, 0.04 s, 0.05 s, 0.06 s, 0.07 s, 0.08 s, 0.09 s, 0.1 s, 0.12 s, 0.14 s, 0.16 s, 0.18 s, 0.2 s, 0.22 s, 0.24 s, 0.26 s, 0.28 s, 0.3 s, 0.35 s,0.4 s, 0.45 s, 0.5 s), after which time most of the magnetization had been lost to relaxation.

Kinetic Modelling of NMR Exchange Data

The integrals of each of the four signals from the above experiments versus time were fitted to the model shown in scheme S1 using a standard Runge-Kutta minimization procedure in the program Berkeley Madonna. The relaxation rates were measured by a standard inversion recovery experiment and fixed to these values during fitting. To conserve 'mass' during data fitting we introduced the fictitious species E, to represent all of the relaxed magnetization. In order to minimize variables, the rate of deinsertion was fixed to the rate of insertion using the equilibrium constant measured previously. Also included in this model are corrections for formation of para-hydrogen. Since para-H_2, which has no NMR signal, accounts for 25% of all H_2 at room temperature, every reaction that makes H_2 will lose 25% magnetization due to formation of para-H_2. In order to fit the data for excitation of the formate or hydride signals of **2**, it was necessary to vary the relaxation time of the excited proton. The fitted value was always somewhat slower than that measured by inversion recovery. We attribute this difference to the contribution of exchange to the relaxation rate measured with inversion recovery (i.e. more slowly relaxing protons (e.g. those in the molecule **2**) are able to exchange into **1**, which relax many times faster).

The fitted rate constants for insertion and deinsertion are shown in Tables 1 and S2. Included in this model, are the rate constants for exchange of RuH_4 and H_2 with each other. However, these rates in reality depend on the concentration of the unobserved intermediate $(P(Ar)_3)_3RuH_2$, and thus are not easily comparable to each other or to other complexes, which undergo similar processes. For system **1d**/**2d**, no exchange occurred between **1d** and **2d**. Therefore, we estimated the upper limit of its deinsertion rate as 5 times slower than the slowest relaxation rate or $< 0.4\ s^{-1}$.

ASSOCIATED CONTENT

Supporting Information

Experimental detail, compound characterization data, NMR spectra, cif file, equilibrium data, exchange measurements and DFT calculation data. The Supporting Information is available free of charge on the ACS Publications website.

AUTHOR INFORMATION

Corresponding Author

walter.leitner@cec.mpg.de
deven.estes@itc.uni-stuttgart.de
d) Current Address: Institute for Chemical Technology, University of Stuttgart, Pfaffenwaldring 55, 70569, Stuttgart, Germany.

Notes

The authors declare no competing financial interests.

ACKNOWLEDGMENTS

The authors would like to thank the Max Planck Society for funding. The authors would also like to thank Drs. John Decatur, Steffen Jockusch, and Christophe Farès and Prof. James Mayer for helpful discussions.

References

(1) a) Many reports use $H_2Ru(PPh_3)_4$ as the Ru precatalyst. However, $H_2Ru(PPh_3)_4$ readily converts to $H_4Ru(PPh_3)_3$ under catalytic conditions as shown in references 1d, 2a, and 2b. In reference 1c, Jessop and coworkers showed that catalyst mixtures with 4:1 P:Ru ratios have the same activities as those with 3:1 P:Ru ratios, suggesting that even when excess phosphine is present, it does not play a major role in catalysis. Thus, we consider $H_4Ru(PR_3)_3$ to be relevant to the catalytic cycles of reactions with $H_2Ru(PR_3)_4$; b) Inoue, Y.; Izumida, H.; Sasaki, Y.; Hashimoto, H., Catalytic Fixation of Carbon Dioxide to Formic Acid by Transition-Metal Complexes Under Mild Conditions. *Chem. Lett.* **1976,** *5*, 863-864; c) Tai, C.-C.; Pitts, J.; Linehan, J. C.; Main, A. D.; Munshi, P.; Jessop, P. G., In Situ Formation of Ruthenium Catalysts for the Homogeneous Hydrogenation of Carbon Dioxide. *Inorg. Chem.* **2002,** *41*, 1606-1614; d) Samouei, H.; Miloserdov, F. M.; Escudero-Adán, E. C.; Grushin, V. V., Solid-State Structure and Solution Reactivity of [(Ph3P)4Ru(H)2] and Related Ru(II) Complexes Used in Catalysis: A Reinvestigation. *Organometallics* **2014,** *33*, 7279-7283; e) Sordakis, K.; Tang, C.; Vogt, L. K.; Junge, H.; Dyson, P. J.; Beller, M.; Laurenczy, G., Homogeneous Catalysis for Sustainable Hydrogen Storage in Formic Acid and Alcohols. *Chem. Rev.* **2018,** *118*, 372-433.

(2) a) Komiya, S.; Yamamoto, A., Reactions of hydrido complexes of ruthenium and rhodium with carbon dioxide involving reversible insertion. *J. Organomet. Chem.* **1972,** *46*, C58-C60; b) Kolomnikov, I. S.; Gusev, A. I.; Aleksandrov, G. G.; Lobeeva, T. S.; Struchkov, Y. T.; Vol'pin, M. E., Structure of the product formed in the reaction of carbon dioxide with ruthenium hydride complexes. *J. Organomet. Chem.* **1973,** *59*, 349-351.
(3) a) Wesselbaum, S.; vom Stein, T.; Klankermayer, J.; Leitner, W., Hydrogenation of Carbon Dioxide to Methanol by Using a Homogeneous Ruthenium–Phosphine Catalyst. *Angew. Chem. Int. Ed.* **2012,** *51*, 7499-7502; b) Wesselbaum, S.; Moha, V.; Meuresch, M.; Brosinski, S.; Thenert, K. M.; Kothe, J.; Stein, T. v.; Englert, U.; Holscher, M.; Klankermayer, J.; Leitner, W., Hydrogenation of carbon dioxide to methanol using a homogeneous ruthenium-Triphos catalyst: from mechanistic investigations to multiphase catalysis. *Chem. Sci.* **2015,** *6*, 693-704; c) Thenert, K.; Beydoun, K.; Wiesenthal, J.; Leitner, W.; Klankermayer, J., Ruthenium-Catalyzed Synthesis of Dialkoxymethane Ethers Utilizing Carbon Dioxide and Molecular Hydrogen. *Angew. Chem. Int. Ed.* **2016,** *55*, 12266-12269.
(4) a) Seibicke, M.; Siebert, M.; Siegle, A. F.; Gutenthaler, S. M.; Trapp, O., Application of Hetero-Triphos Ligands in the Selective Ruthenium-Catalyzed Transformation of Carbon Dioxide to the Formaldehyde Oxidation State. *Organometallics* **2019,** *38*, 1809-1814; b) Siebert, M.; Krennrich, G.; Seibicke, M.; Siegle, A. F.; Trapp, O., Identifying high-performance catalytic conditions for carbon dioxide reduction to dimethoxymethane by multivariate modelling. *Chem. Sci.* **2019,** *10*, 10466-10474; c) Siebert, M.; Seibicke, M.; Siegle, A. F.; Kräh, S.; Trapp, O., Selective Ruthenium-Catalyzed Transformation of Carbon Dioxide: An Alternative Approach toward Formaldehyde. *J. Am. Chem. Soc.* **2019,** *141*, 334-341.
(5) Loges, B.; Boddien, A.; Junge, H.; Beller, M., Controlled Generation of Hydrogen from Formic Acid Amine Adducts at Room Temperature and Application in H2/O2 Fuel Cells. *Angew. Chem. Int. Ed.* **2008,** *47*, 3962-3965.
(6) a) Aresta, M.; Dibenedetto, A.; Angelini, A., Catalysis for the Valorization of Exhaust Carbon: from CO2 to Chemicals, Materials, and Fuels. Technological Use of CO2. *Chem. Rev.* **2014,** *114*, 1709-1742; b) Eppinger, J.; Huang, K.-W., Formic Acid as a Hydrogen Energy Carrier. *ACS Energ. Lett.* **2017,** *2*, 188-195.
(7) a) Preti, D.; Resta, C.; Squarcialupi, S.; Fachinetti, G., Carbon Dioxide Hydrogenation to Formic Acid by Using a Heterogeneous Gold Catalyst. *Angew. Chem. Int. Ed.* **2011,** *50*, 12551-12554; b) Wesselbaum, S.; Hintermair, U.; Leitner, W., Continuous-Flow Hydrogenation of Carbon Dioxide to Pure Formic Acid using an Integrated scCO2 Process with Immobilized Catalyst and Base. *Angew. Chem.* **2012,** *124*, 8713-8716; c) Jens, C. M.; Scott, M.; Liebergesell, B.; Westhues, C. G.; Schäfer, P.; Franciò, G.; Leonhard, K.; Leitner, W.; Bardow, A., Rh-Catalyzed Hydrogenation of CO2 to Formic Acid in DMSO-based Reaction Media: Solved and Unsolved Challenges for Process Development. *Adv. Syn. Catal.* **2019,** *361*, 307-316.
(8) a) Jessop, P. G.; Ikariya, T.; Noyori, R., Homogeneous Hydrogenation of Carbon Dioxide. *Chem. Rev.* **1995,** *95*, 259-272; b) Leitner, W., Carbon Dioxide as a Raw Material: The Synthesis of Formic Acid and Its Derivatives from CO2. *Angew. Chem. Int. Ed.* **1995,** *34*, 2207-2221; c) Wang, W.-H.; Himeda, Y.; Muckerman, J. T.; Manbeck, G. F.; Fujita, E., CO2 Hydrogenation to Formate and Methanol as an Alternative to Photo- and Electrochemical CO2 Reduction. *Chem. Rev.* **2015,** *115*, 12936-12973.
(9) a) Fulmer, G. R.; Herndon, A. N.; Kaminsky, W.; Kemp, R. A.; Goldberg, K. I., Hydrogenolysis of Palladium(II) Hydroxide, Phenoxide, and Alkoxide Complexes. *J. Am. Chem. Soc.* **2011,** *133*, 17713-17726; b) Webb, J. R.; Burgess, S. A.; Cundari, T. R.; Gunnoe, T. B., Activation of carbon–hydrogen bonds and dihydrogen by 1,2-CH-addition across metal–heteroatom bonds. *Dalton Trans.* **2013,** *42*, 16646-16665.
(10) Grasemann, M.; Laurenczy, G., Formic acid as a hydrogen source – recent developments and future trends. *Energ. Env. Sci.* **2012,** *5*, 8171-8181.
(11) Chaudret, B.; Poilblanc, R., Preparation of polyhydride complexes of ruthenium by direct hydrogenation of zerovalent olefinic derivatives. Mononuclear complexes of the type RuH6L2 and RuH4L3. Spontaneous hydrogen-deuterium exchange between the phosphine protons and the solvent catalyzed by RuH4L3. *Organometallics* **1985,** *4*, 1722-1726.
(12) Knoth, W. H., Dihydrido(dinitrogen)tris(triphenylphosphine)ruthenium. Dinitrogen bridging ruthenium and boron. *J. Am. Chem. Soc.* **1972,** *94*, 104-109.
(13) Gunanathan, C.; Capelli, S. C.; Englert, U.; Hölscher, M.; Leitner, W., Structures and Dynamics of the Mixed Dihydrogen/Hydride Complexes [Ru(PCP)(H)(H2)n] (n = 1, 2) and [Ru(PNP)(H)2(H2)]. *Eur. J. Inorg. Chem.* **2013,** *2013*, 5075-5080.
(14) Luo, X. L.; Crabtree, R. H., Testing the T1 method: a comparison of T1(min) and structural data. *Inorg. Chem.* **1990,** *29*, 2788-2791.
(15) Jeletic, M. S.; Hulley, E. B.; Helm, M. L.; Mock, M. T.; Appel, A. M.; Wiedner, E. S.; Linehan, J. C., Understanding the Relationship Between Kinetics and Thermodynamics in CO2 Hydrogenation Catalysis. *ACS Catal.* **2017,** *7*, 6008-6017.
(16) a) Hazari, N.; Heimann, J. E., Carbon Dioxide Insertion into Group 9 and 10 Metal–Element σ Bonds. *Inorg. Chem.* **2017,** *56*, 13655-13678; b) Heimann, J. E.; Bernskoetter, W. H.; Guthrie, J. A.; Hazari, N.; Mayer, J. M., Effect of Nucleophilicity on the Kinetics of CO2 Insertion into Pincer-Supported Nickel Complexes. *Organometallics* **2018,** *37*, 3649-3653; c) Heimann, J. E.; Bernskoetter, W. H.; Hazari, N.; Mayer, James M., Acceleration of CO2 insertion into metal hydrides: ligand, Lewis acid, and solvent effects on reaction kinetics. *Chem. Sci.* **2018,** *9*, 6629-6638.
(17) Ramakrishnan, S.; Waldie, K. M.; Warnke, I.; De Crisci, A. G.; Batista, V. S.; Waymouth, R. M.; Chidsey, C. E. D., Experimental and Theoretical Study of CO2 Insertion into Ruthenium Hydride Complexes. *Inorg. Chem.* **2016,** *55*, 1623-1632.
(18) Waldie, K. M.; Brunner, F. M.; Kubiak, C. P., Transition Metal Hydride Catalysts for Sustainable Interconversion of CO2 and Formate: Thermodynamic and Mechanistic Considerations. *ACS Sus. Chem. Eng.* **2018,** *6*, 6841-6848.
(19) a) Mondal, B.; Neese, F.; Ye, S., Control in the Rate-Determining Step Provides a Promising Strategy To Develop New Catalysts for CO2 Hydrogenation: A Local Pair Natural Orbital Coupled Cluster Theory Study. *Inorg. Chem.* **2015,** *54*, 7192-7198; b) Mondal, B.; Neese, F.; Ye, S., Toward Rational Design of 3d Transition Metal Catalysts for CO2 Hydrogenation Based on Insights into Hydricity-Controlled Rate-Determining Steps. *Inorg. Chem.* **2016,** *55*, 5438-5444.
(20) Sawatlon, B.; Wodrich, M. D.; Corminboeuf, C., Unraveling Metal/Pincer Ligand Effects in the Catalytic Hydrogenation of Carbon Dioxide to Formate. *Organometallics* **2018,** *37*, 4568-4575.
(21) Kessler, H.; Mronga, S.; Gemmecker, G., Multi-dimensional NMR experiments using selective pulses. *Mag. Res. Chem.* **1991,** *29*, 527-557.
(22) Macey, R.; Oster, G. *Berkeley Madonna*, 9.1.14; 2018.
(23) Since the excited proton has a net magnetization, during the de-insertion, it will combine with the unmagnetized coupling partner to make a thermodynamic mixture of ortho- and para-H_2 (75% and 25% at room temperature, respectively). Since para-H_2 is NMR silent, making para-H_2 represents overall magnetization loss and must be taken into account in our differential equations. See Scheme S1 for details.
(24) a) Tsai, J. C.; Nicholas, K. M., Rhodium-catalyzed hydrogenation of carbon dioxide to formic acid. *J. Am. Chem. Soc.* **1992,** *114*, 5117-5124; b) Hutschka, F.; Dedieu, A.; Eichberger, M.; Fornika, R.; Leitner, W., Mechanistic Aspects of the Rhodium-Catalyzed Hydrogenation of CO2 to

Formic AcidA Theoretical and Kinetic Study. *J. Am. Chem. Soc.* **1997,** *119,* 4432-4443; c) Urakawa, A.; Jutz, F.; Laurenczy, G.; Baiker, A., Carbon Dioxide Hydrogenation Catalyzed by a Ruthenium Dihydride: A DFT and High-Pressure Spectroscopic Investigation. *Chemistry – A European Journal* **2007,** *13,* 3886-3899.

(25) Pertici, P.; Vitulli, G.; Spink, W. C.; Rausch, M. D., Cycloolefin Complexes of Ruthenium. *Inorg. Synth.* **1983,** *22,* 176-181.

(26) Raiford, D. S.; Fisk, C. L.; Becker, E. D., *Anal. Chem.* **1979,** *51,* 2050-2051.

(27) a) Kessler, H.; Oschkinat, H.; Griesinger, C.; Bermel, W., *J. Mag. Res.* **1986,** *70,* 106-133; b) Stonehouse, J.; Adell, P.; Keeler, J.; Shaka, A. J., *J. Am. Chem. Soc.* **1994,** *116,* 6037-6038; c) Stott, K.; Keeler, J.; Van, Q. N.; Shaka, A. J., *J. Mag. Res.* **1997,** *125,* 302-324.

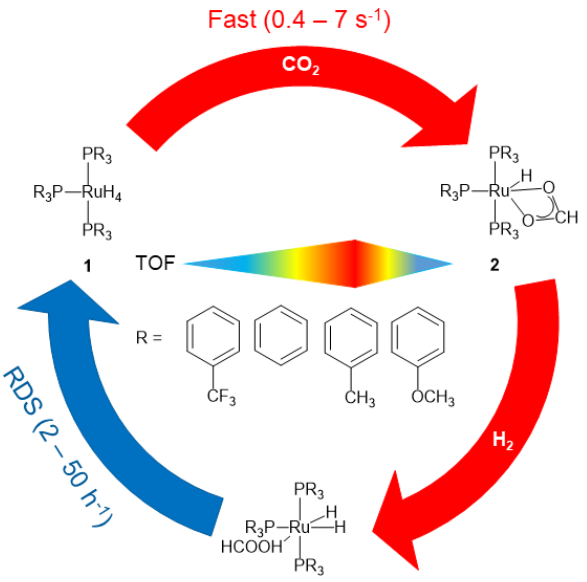
Fast (0.4 – 7 s-1)
CO2
PR3
R3P—RuH4
PR3
1
TOF
PR3
R3P—Ru
H
O
O=CH
PR3
2
R =
CF3
CH3
OCH3
H2
RDS (2 – 50 h-1)
PR3
R3P—Ru—H
HCOOH
PR3

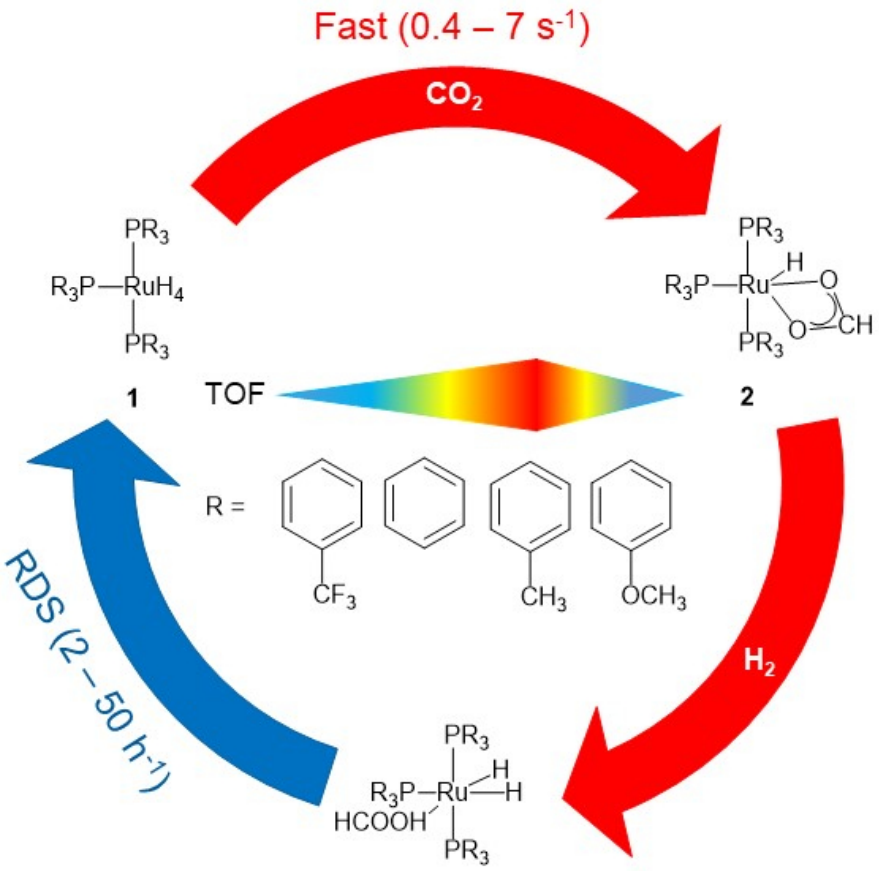
Fast (0.4 – 7 s-1)
CO2
PR3
R3P—RuH4
PR3
1
TOF
PR3
R3P—Ru
H
O
O=CH
PR3
2
R =
CF3
CH3
OCH3
H2
RDS (2 – 50 h-1)
PR3
R3P—Ru—H
HCOOH
PR3

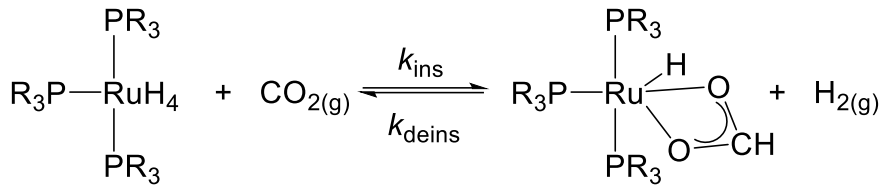

1b **2b**

2b-hydride

2b-formate

H_2

1b

8 6 4 2 0 -2 -4 -6 -8 -10 -12 -14 -16 -18 ppm

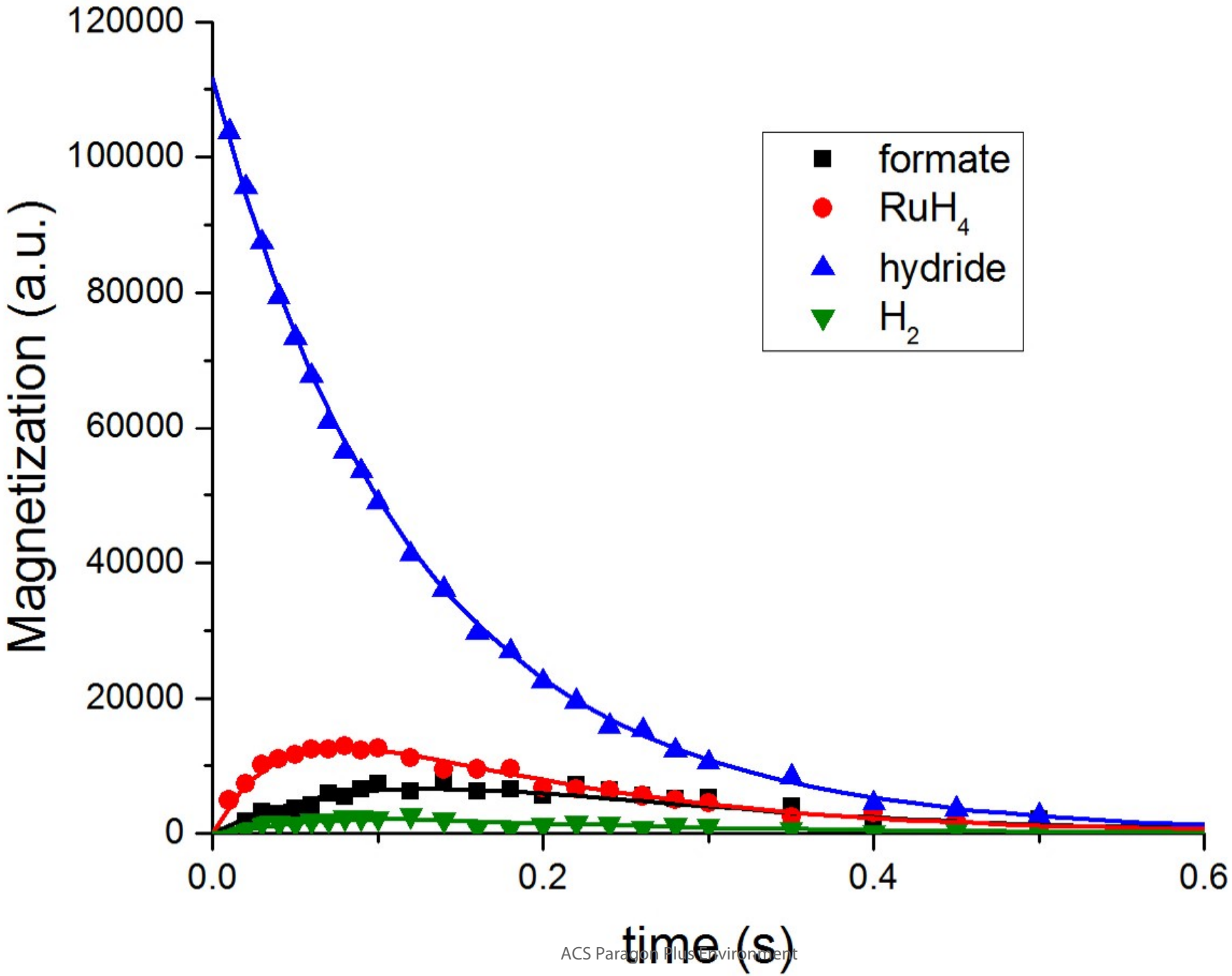
120000
100000
80000
60000
40000
20000
0
Magnetization (a.u.)
0.0
0.2
0.4
0.6
time (s)
formate
RuH4
hydride
H2